Journal of Materials Chemistry B

PAPER

View Article Online
View Journal | View Issue

Cite this: J. Mater. Chem. B, 2019, 7, 7235

Synthesis of new multivalent metal ion functionalized mesoporous silica and studies of their enhanced antimicrobial and cytotoxicity activities

Suman Chirra,[a] Suresh Siliveri,[a] Ravi Gangalla,[b] Srinath Goskula,[a] Sripal Reddy Gujjula,[a] Ajay Kumar Adepu,[c] Rajini Anumula,[d] Siva Sankari Sivasoorian,[e] Li-Fang Wang[e] and Venkatathri Narayanan *[a]

In the present study, we have reported the synthesis of a transition metal (Me = Ti, V, and Pd) incorporated into MCM-41 mesoporous molecular sieves (Si/Me = 20) synthesized by the sol–gel method. Their physicochemical properties were studied in detail by standard techniques like low angle powder X-ray diffraction (XRD), scanning electron microscopy-energy-dispersive X-ray spectroscopy (SEM-EDXS), transmission electron microscopy (TEM), N_2 adsorption/desorption studies, and thermogravimetric-differential thermal (TG-DTA) analysis and spectral studies like Fourier transform infrared spectroscopic analysis (FT-IR), diffuse reflectance ultraviolet-visible spectroscopic analysis (UV-Visible-DRS), and X-ray photoelectron spectroscopy (XPS). The XRD patterns prove that the material's phase identity is the same irrespective of metal incorporation. SEM displayed the uniform shape and size of the nanoparticles. The presence of elements such as Ti, V, Pd, Si and O in respective materials is revealed using the EDXS analysis. Around 30% weight loss arose upon calcination from room temperature to 800 °C. BET surface area analysis presented that the parent materials have a high surface area (1024 m^2 g^{-1}) which was reduced upon metal incorporation. FT-IR analysis exhibited the framework vibrations of the synthesised materials. UV-Visible-DRS analysis indicated the presence of tetrahedrally coordinated transition metal ions. The multivalent-metal-ion-functionalized mesoporous materials showed significant enhancement in potent antimicrobial and anticancer activity. The antimicrobial activity is because of its low lipophilicity, which no longer allows the materials to enter *via* the lipid membrane. Thus, the new materials neither obstruct the metal-binding sites nor inhibit the growth of microbe enzymes. Further, the results show that the transition metal ion-containing mesoporous materials possessing good anticancer activity arising from their excessive surface area to volume ratio provided appropriate association with a tumour cell due to the direct penetration of mesoporous materials into the cell wall, causing membrane damage and cell death.

Received 14th August 2019,
Accepted 11th October 2019

DOI: 10.1039/c9tb01736d

rsc.li/materials-b

1. Introduction

Due to the outstanding structural features of mesoporous compounds, such as large surface area, pore volume, ordered and uniform pore networks with even and precise pore architecture, facile surface functionalities, stable physicochemical behavior, superior mechanical strength and thermal stability, they have been found to be promising materials for various applications[1–4] in many areas of technology, such as gas storage, catalysis, adsorption/separation, sensors, chromatography, solar cells, optoelectronics, light-harvesting[5–13] and other essential areas of science. Mesoporous materials are biocompatible and non-toxic; this fantastic property offers these materials applicability in biotechnology, including their role as biomaterials for sensing, drug delivery and bone tissue regeneration technologies.[14–16] Extreme efforts have been made to engineer multiple transition element-incorporated porous silicate frameworks to modify the structure, catalytic behaviour and physicochemical properties of the

[a] Department of Chemistry, National Institute of Technology, Warangal 506 004, Telangana, India. E-mail: venkatathrin@yahoo.com; Tel: +91-9491319976
[b] Department of Microbiology, Kakatiya University, Warangal 506 009, Telangana, India
[c] Inorganic & Physical Chemistry Division, CSIR – Indian Institute of Chemical Technology, Hyderabad 500007, India
[d] State Key Laboratory for Structural Chemistry of Unstable and Stable Species, Institute of Chemistry, Chinese Academy of Sciences, Beijing 100090, China
[e] Department of Medicinal & Applied Chemistry, College of Life Science, Kaohsiung Medical University, Kaohsiung 807, Taiwan

mesoporous matrices. Due to the low toxicity of silica-based porous materials and their capability to host a range of fluorescent indicators, dyes and drugs, they can be used to track the location of therapeutic agents and their activity.[17–23] Mesoporous materials are attractive tools for anti-cancer treatment. The use of mesoporous materials as anti-cancer drug vehicles can possibly enrich the cytotoxicity of chemotherapeutic agents with improved efficiency in targeting the malignant tissues rather than healthy tissues.[24] The problem of targeting healthy cells instead of cancer cells can be tackled with the use of mesoporous materials along with chemotherapeutic agents. Mesoporous silica materials have been tested before use for bio-applications.[25–32] The current research trends in modern science involve incorporating single or multiple metal ions into porous structured materials. From past literature, it was found that mesoporous silica materials containing different metal and metal oxides were widely studied and they were found to be eco-friendly, and hence used widely in multiple industries in various catalytic transformations.[33] Mesoporous silica has been used as a support for different metals due to its unique characteristic features, such as the flexibility of its tetrahedrally coordinated silicon atoms and accurate control of its hydrolysis condensation, allowing for more thermal stability and lower reactivity. Also, the metals and heteroatoms incorporated inside the framework are stabilised and increase the fixing capacity toward different functional groups.[34,35] The above special features favour mesoporous silica for multiple catalytic applications.

As platinum group metals are expensive and hard to obtain at a low price, researchers have been targeting non-platinum groups in advanced anticancer research. Few researchers have also focused on various transition metals for biotic purposes. Recent studies on the non-platinum group metals have explained the exhibition of noticeable *in vivo* and *in vitro* activities in counter to several tumour cells. Compounds based on transition metals such as vanadium (V), titanium (Ti), copper (Cu), ruthenium (Ru), tin (Sn) and rhodium (Rh) have proved to possess chemotherapeutic potential. Of these transition metal-based compounds, vanadium compounds have been recognised to accomplish therapeutic applications, such as anti-diabetic, anti-HIV, and anticancer properties, and are also concerned in various biological developments, like cell growth. The transition metal complexes of Ti, V, Fe, Au, Ru, Sn, and Mo have been revealed to have *in vivo* and *in vitro* antitumor activity, but Ru and Ti have been most effective, gathering collective interest for clinical trials. Because of the lesser harm and smaller quantity of critical aspect outcomes shown by Ti(IV) materials compared to different transition metals, Ti(IV) substances are exceptional options for therapeutic applications.[36–38] From recent research trends, there have been many remarkable improvements in the anti-cancer chemistry of palladium-based mesoporous materials. Palladium(II) compounds are isoelectronic and isostructural with platinum(II) and are prominent potential anticancer agents; in some cases, they have been more active than cisplatin.[39] The present work employs synthesis of Ti-, V-, and Pd-metal-ion-functionalized mesoporous materials through the sol–gel method, detailed characterisation of the synthesised materials using different physicochemical techniques, and studies of their anti-microbial and anti-cancer activities.

2. Experimental section

2.1. Materials and methods

Synthesis of pure siliceous mesoporous molecular sieve material was executed in a glass beaker by a modified sol–gel method.[40,41] In this unique synthesis, 2.40 g of surfactant cetyltrimethylammonium bromide (CTAB, $CH_3(CH_2)_{15}N(CH_3)_3Br$, 99%, Sigma-Aldrich) was liquefied in 50.00 mL of double-distilled water (DDW) and constantly stirred to form a clear homogeneous solution. To 13.00 mL of 25 wt% aqueous ammonia (Merck), 76.00 mL of ethyl alcohol (Merck) was added. At the same time, 10.00 mL of tetraethylorthosilicate (TEOS, 99.9%, Sigma-Aldrich) was added dropwise to the above mixture while stirring. The solution turned milky and a gel formed because of the hydrolysis of TEOS. The solution was stirred for about two hours to hydrolyse TEOS completely. The formed white precipitate was centrifuged and washed repeatedly with double distilled water (DDW) and methanol. The product desiccated in the air overnight at 110 °C. The resultant product was calcined at 550 °C in the air for five hours to eradicate the surfactant. Metal ion functionalized mesoporous silica was synthesised by following the same method as defined for mesoporous silica with the addition of suitable quantities (Si/M ion ratio of 100) of metal precursors 20 minutes after TEOS was added. Titanium tetraisopropoxide, vanadyl acetylacetonate and palladium acetate were used as Ti, V, and Pd sources, respectively.

2.2 Sample characterization

The low-angle powder X-ray diffraction patterns were recorded on an Ultima IV diffractometer (M/s, Rigaku Corporation, Japan) with Ni-filtered Cu Kα radiation (λ = 1.54178 Å) at 30 mA and 40 kV and within the 2θ range of 0.1–5° with a step size of 0.008° and a scan rate of 0.5° per minute. Transmission electron microscopy (TEM) images of the samples were analysed using a JEOL JEM2100 TEM instrument (Australia) with an acceleration voltage of 200 kV. The surface morphological studies and elemental analysis (SEM/E-DAX) were carried out using a scanning electron microscope (TESCAN, VEGA 3 LMU instrument, South Korea). An STA 2500 Regulus NETZSCH instrument (Japan) was used for the thermogravimetry-differential thermal analysis (TG-DTA) studies. The pore size and surface area characteristics of the samples were characterised under liquid nitrogen at 77 K using a Quanta Chrome Nova-1000 (USA) surface analyser instrument; the de Boer *t*-plot and Brunauer–Emmett–Teller (BET) methods were used to determine pore volume and surface area, respectively. Fourier transform infrared spectra (FT-IR) samples were recorded (PerkinElmer, Spectrum 100, USA) using 1 : 10 KBr pellets for 10 scans at room temperature. Ultraviolet-visible diffuse reflectance (UV-Vis-DRS) spectra of the samples were recorded on a Thermo Scientific Evolution 300 UV-Visible spectrophotometer (USA) with $BaSO_4$ reference. X-ray photoelectron spectroscopic (XPS)

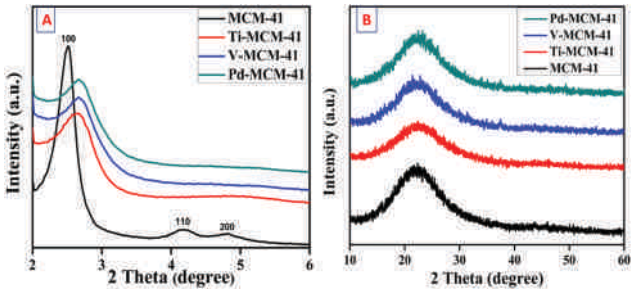

Fig. 1 (A) Low angle and (B) wide-angle X-ray diffraction patterns of mesoporous silica and transition metal ion functionalized mesoporous silica.

analysis was performed using a Thermo Fisher Scientific Theta Probe Spectrometer (East Grinstead, UK) for elemental quantification.

2.3 Anti-microbial activity

0.5 mL of 24 h-old bacterial culture was spread on a plate and in wells filled with either 600 μg mL^{-1} or 900 μg mL^{-1} MCM-41, Ti-MCM-41, V-MCM-41 and Pd-MCM-41 compounds, followed by incubation at 25 °C. After 24 h, good diffusion was observed and the anti-microbial activity was measured. NAM plots were prepared for two Gram-negative (*Escherichia coli*, *Salmonella paratyphi*) and two Gram-positive (*Bacillus subtilis*, *Staphylococcus aureus*) bacteria. Zone of inhibition (ZOI) were calculated using the HI antibiotic zone scale.

2.4 Cell culture and cell viability analysis

Human chronic myeloid leukaemia cell line K562 cultivated in RPMI1640 (Lonza, India) was complemented with 10% fetal bovine serum (FBS) (Hi-Media, India) and antibiotics (Lonza, India).

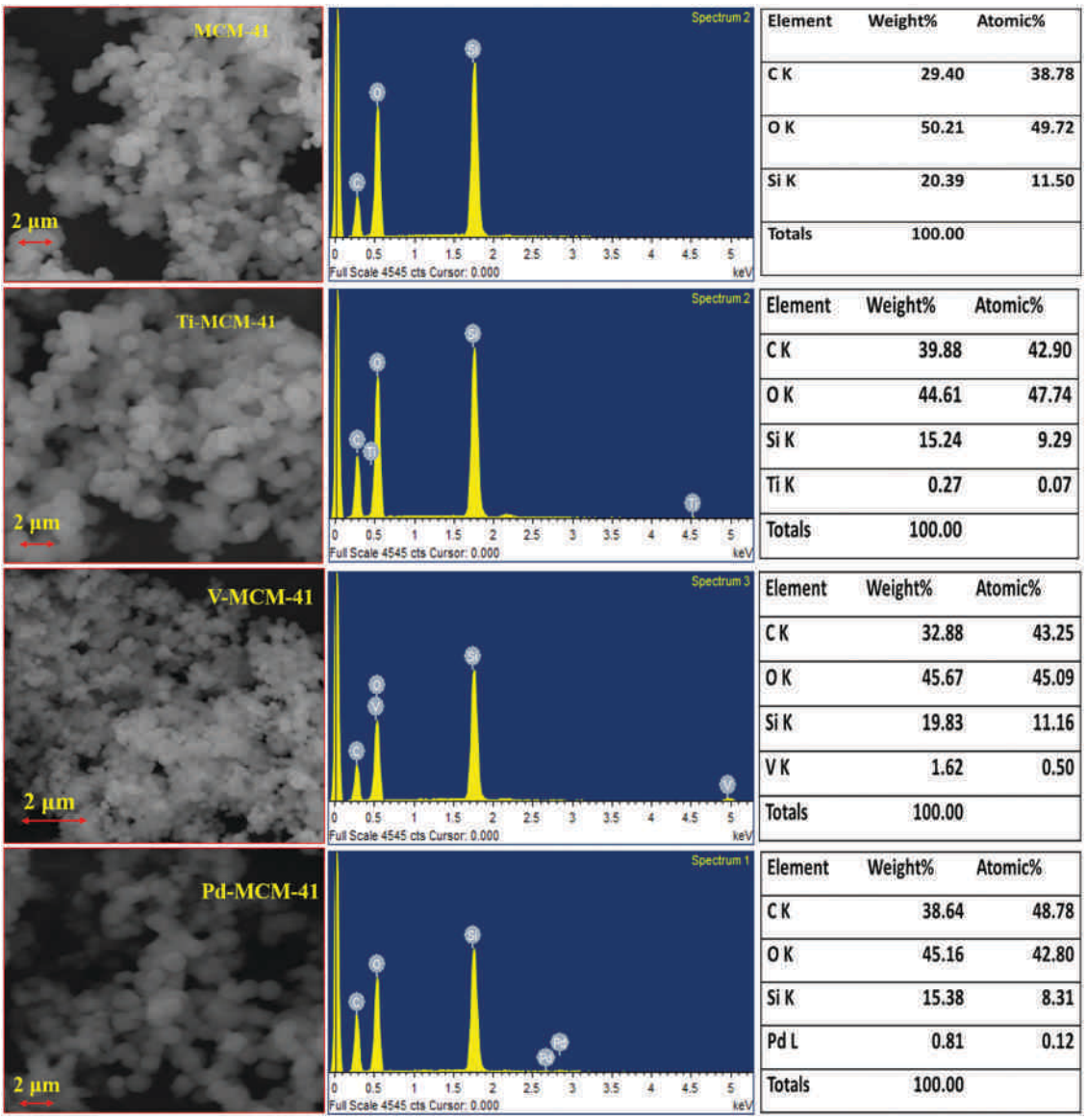

Fig. 2 Scanning electron micrographs of the types of mesoporous silica materials and their elemental analysis.

Adherent cell lines HeLa and MCF7 were cultivated in Dulbecco's Modified Eagle Medium (DMEM) medium (Lonza, India) supplemented with 10% FBS (Hi-Media, India) and antibiotics (Lonza, India). To assess cell viability, HeLa and MCF7 cells were cultured at 2000 cells per well and K562 Cells were cultured at 5000 cells per well in a 96-well plate. A stock solution of silica nanoparticles was prepared at 20 mg ml^{-1} in DMSO and cells were treated in triplicate with concentrations of 10 μg mL^{-1}, 20 μg mL^{-1}, 50 μg mL^{-1}, and 100 μg mL^{-1}. After 48 hours, cell viability was assessed using Alamar blue reagent (BioSource, India) using a Bio-Rad plate reader.[42] For morphological assessment, HeLa and MCF7 cells were cultured at 10 000 cells per well and treated with 10 μg mL^{-1} and 25 μg mL^{-1} of particles for 48 h. Untreated cells were taken as a control and all cells were imaged under the light microscope at a magnification of 20×.

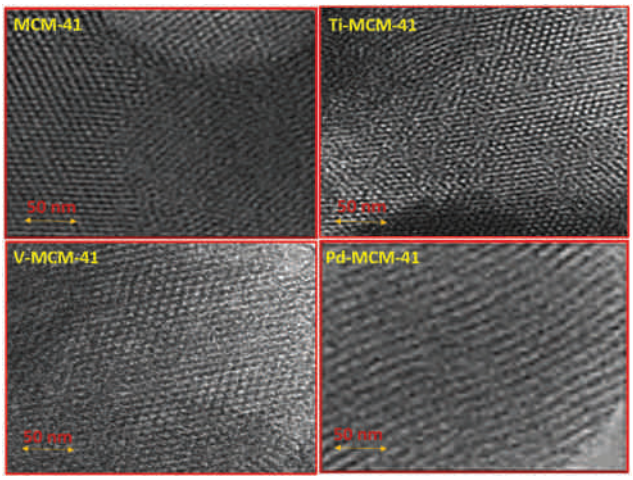

Fig. 3 Transmission electron micrographs of various types of MS molecular sieves (MCM-41 = MS).

3. Results and discussion

3.1. X-ray diffraction pattern

The X-ray diffraction (XRD) patterns of MS and MeMS (Me = Ti^{4+}, V^{5+}, and Pd^{2+}) samples showed only one low-angle peak for the d_{100} plane at the 2θ value of 2.2° corresponding to the mesophase (Fig. 1).[43] This result is characteristic of the long-range hexagonal structure of MS. In the case of metal-incorporated MS, the intensity of the peak is lower than that of the pure MS, suggesting that the existence of metal ions obstructs the structure-directing action of the template and varies the order of materials. The inclusion of titanium into the structure of mesoporous materials is indicated by the low angle peak, showing the occupancy of the metal ion in place of Si ion. Some of the surface Si ions were replaced isomorphously by the guest metal ions.

3.2. Scanning electron microscopy/energy dispersive X-ray analysis

The SEM-EDAX images revealed a spherical morphology with uniform particle size for MS, Ti-MS, V-MS and Pd-MS (Fig. 2). The presence of metal ions in the framework was confirmed by EDAX results,[44] indicating that the morphology remains unaltered even after the incorporation of various metal ions (Fig. 2).

3.3. Transmission electron microscopy

TEM images of calcined MS, Ti-MS, V-MS, and Pd-MS are shown in Fig. 3. The corresponding micrographs unveiled the presence

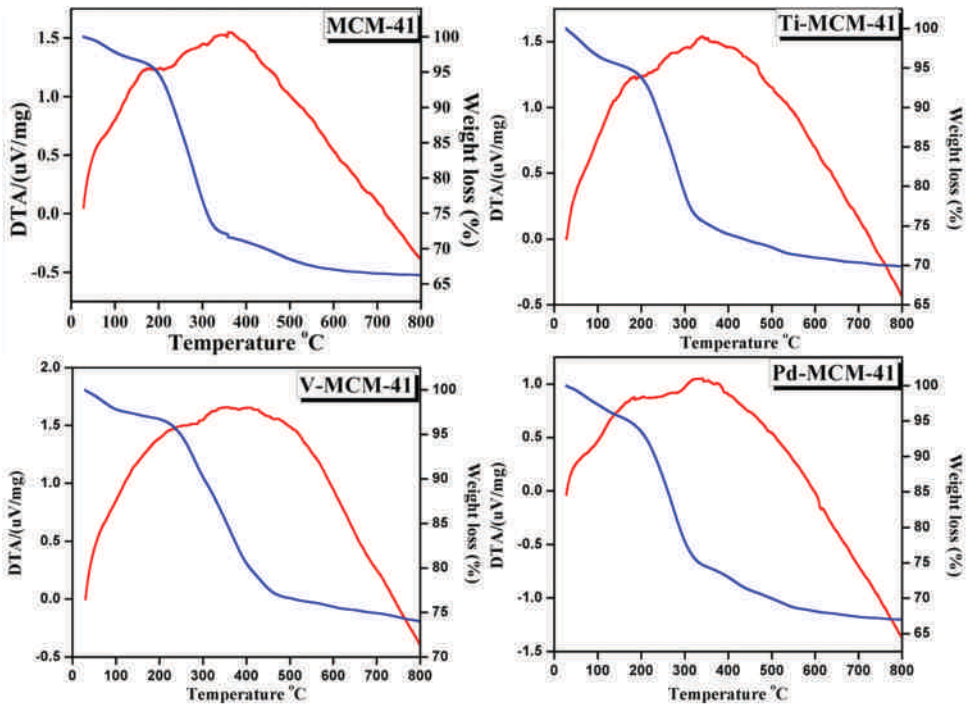

Fig. 4 Thermogravimetric/differential thermal analysis of various types of MS molecular sieves.

Table 1 Thermogravimetric endo- and exothermic weight loss of various mesoporous materials

Mesoporous materials	Endothermic weight loss (25–150 °C)	Exothermic weight loss (151–350 °C)	Exothermic weight loss (351–550 °C)	Residual mass (%)	Total weight loss (%)
MCM-41	3.1	24.3	6.4	66.3	33.8
Ti-MCM-41	3.9	20.4	5.9	69.9	30.2
V-MCM-41	2.5	19.9	3.6	74.0	26.0
Pd-MCM-41	3.7	19.3	10.0	67.0	33.0

of well-defined and ordered channels of characteristic fringes and uniform hexagonal arrangements visible in all of the micrographs. All four figures show a well-developed long-range order of hexagonal structures and a regular two-dimensional hexagonal pore structure for all the samples. The TEM images verify that the Ti-MS nanoparticles are clean segments with tiny and well-ordered mesoporous channels. The small shaded spots demonstrate that Ti has particle sizes around 3 nm and 6 nm.[45] It is suggested that most of the Ti, V, and Pd atoms are outnumbered by the Si atoms in the framework of the MS structure, as those atoms could not be identified in TEM images.[46]

3.4. Thermogravimetry/differential thermal analysis

The as-synthesized MS (Fig. 4a (MS), Fig. 4b (Ti-MS), Fig. 4c (V-MS) and Fig. 4d (Pd-MS)) revealed distinct weight losses for various metal incorporations when analysed by thermogravimetry/differential thermal analysis. It was observed that when the metal substance increases, there is a reduction in organic substance and an increase in water substance. Thus, weight loss was higher in the low-metal substance of MS compared to the high-metal substance. The TG/DTA profiles of the siliceous MS in nitrogen atmosphere showed three distinct stages of weight loss observed in the temperature ranges 50–150 °C, 150–350 °C and 350–550 °C. The first weight loss observed at

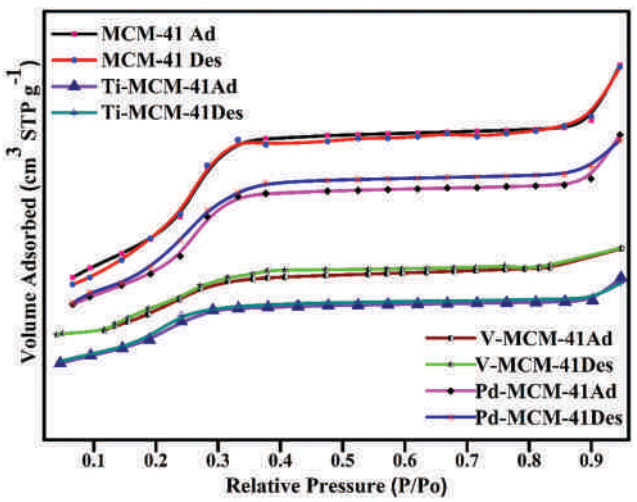

Fig. 5 N_2 adsorption and desorption curves of various calcined MS molecular sieves.

Table 2 Textural properties of various MCM-41 molecular sieves

Material	S_{BET} (m^2 g^{-1})	Pore size (Å)	Pore volume (cc g^{-1})
MCM-41	1023.5	17.2	0.28
Ti-MCM-41	942.3	16.6	0.24
V-MCM-41	831.23	15.8	0.15
Pd-MCM-41	731.12	16.3	0.18

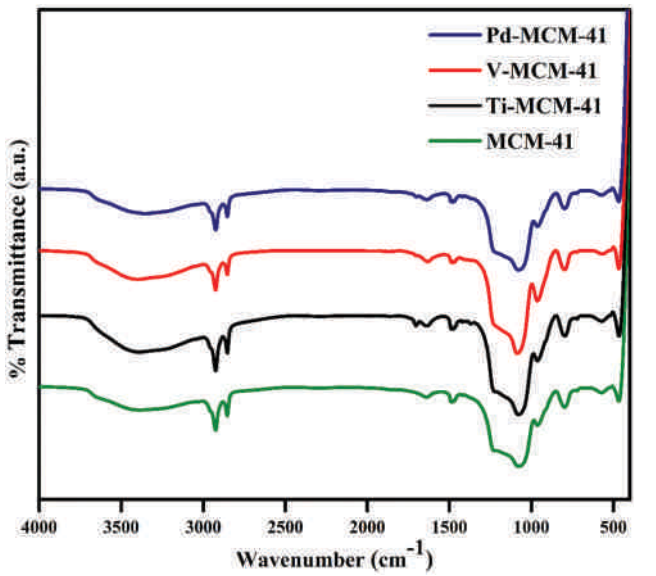

Fig. 6 Fourier transform infrared spectra of various calcined MS molecular sieves.

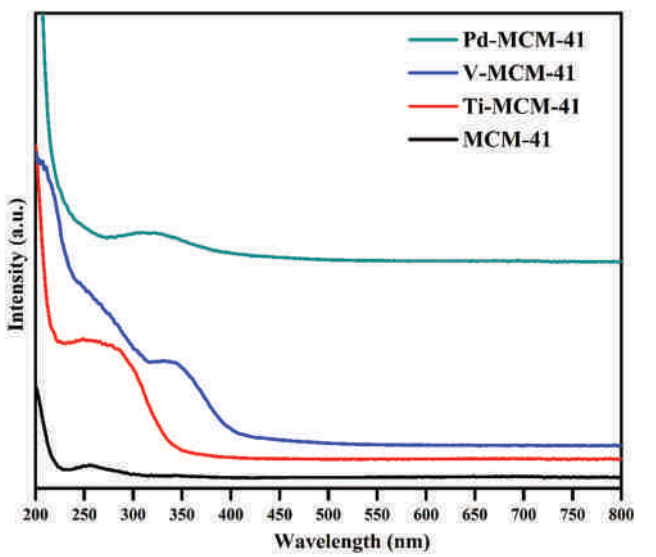

Fig. 7 Diffuse reflectance-ultraviolet-visible spectra of various calcined MS molecular sieves.

50–150 °C is due to desorption of physisorbed water and ethanol occluded inside the mesopores.[47] The binary weight loss seen in the range of 150–350 °C was attributed to the oxidative disintegration of the template.[48] The final weight loss in the temperature range 330–550 °C is the decomposition of leftover surfactant and loss of condensed water. After 550 °C, there was no exothermal peak, which indicates that the template was eradicated at this stage. The textural characteristics of these materials are listed in Table 1.

3.5. BET-surface area

The nitrogen adsorption–desorption isotherms of MS materials are displayed in Fig. 5. The surface areas of different calcined MS materials were calculated from a BET adsorption isotherm. It was noticed that the adsorption follows a typical type-IV adsorption isotherm, indicating mesoporosity.[49] The surface areas of the metal-containing MS are found to decrease with the incorporation of metals (Table 2). Pore size and pore volumes decreased slightly upon metal incorporation in MS. Low angle powder XRD results support this observation.

3.6. Fourier transform infrared spectroscopic analysis

The Fourier transform infrared spectra of MS and metal-incorporated MS are shown in Fig. 6. The FT-IR spectra of pure MS samples showed absorption bands at 1643 cm^{-1} and 3408 cm^{-1} for hydroxyl groups[50–52] and asymmetric stretching vibrations at 1072 cm^{-1} and 1228 cm^{-1} for Si–O–Si bond linkages. The band at around 964 cm^{-1} is ascribed to Si–OH vibrations. The band at 794 cm^{-1} resembles that of free silica and the absorption peaks around 450 to 795 cm^{-1} are mostly

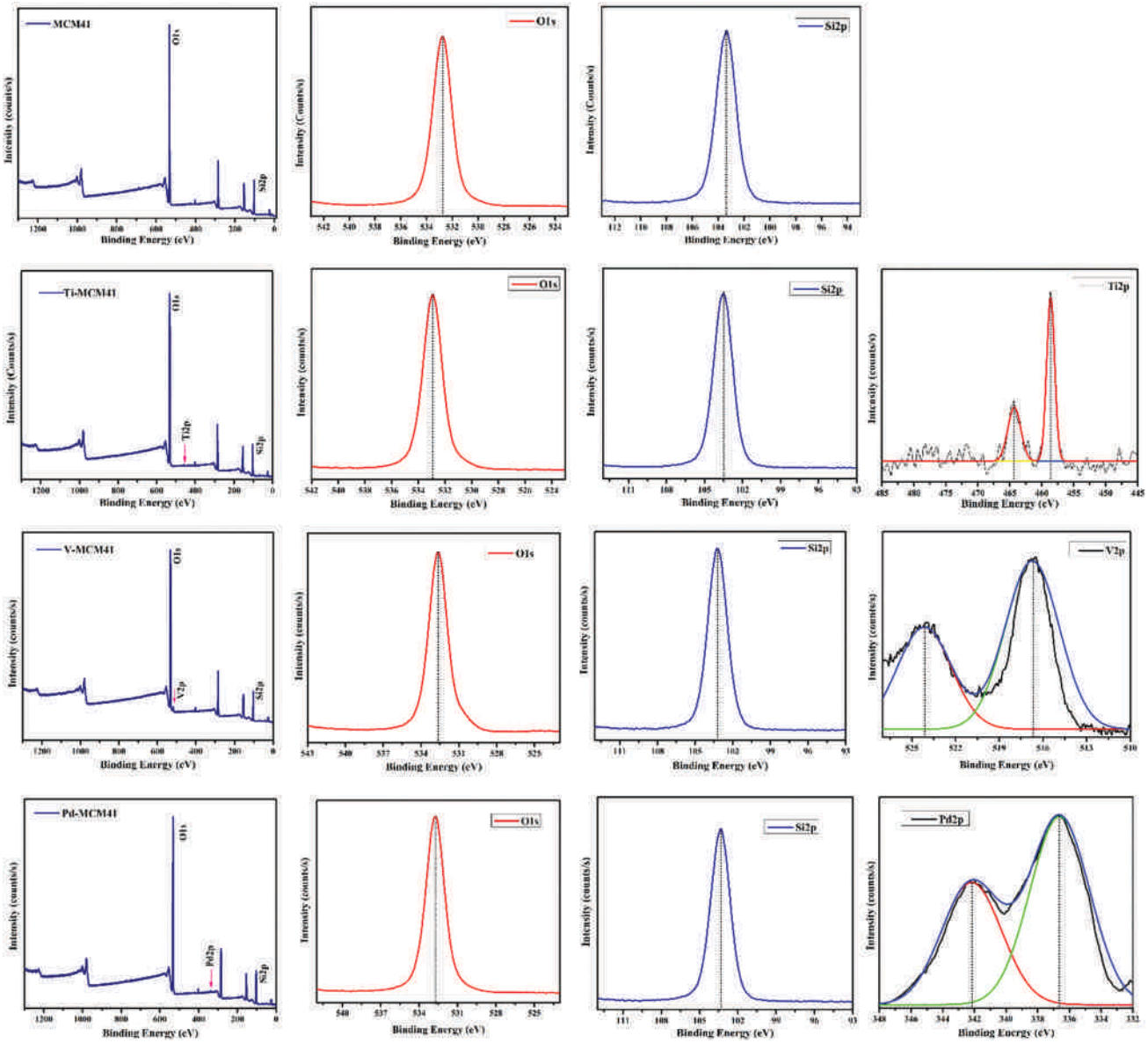

Fig. 8 X-ray photoelectron spectra of various MS type molecular sieves.

due to bending vibrations of Si–O–Si bonds. The uncalcined MS sample displays a shallow intense band at 2926 cm^{-1},[53] related to the C–H stretching of the hydrocarbon chain of the surfactant. In the case of calcined mesoporous materials, the peaks corresponding to C–H stretching vibrations disappeared, indicating the complete removal of template cetyltrimethylammonium bromide from the framework.

3.7. Diffuse reflectance ultraviolet-visible spectroscopy

The ultraviolet-visible spectra of various MS type molecular sieves revealed a band centred at 210 nm (Fig. 7) which was ascribed to a low-energy charge-transfer transition. The band in the range of 260–280 nm suggests the existence of small quantities of polymerised M–O–M types in higher co-ordination co-existing through the tetrahedral metal sites.[54] The absence of an absorption band distinguishing a new octahedral framework metal at approximately 600 nm in samples indicates that there are no separate octahedral species.

3.8. X-ray photoelectron spectroscopy analysis

The surface composition and interaction between general elements in the MCM-41, Ti-MCM-41, V-MCM-41 and Pd-MCM-41 structures were characterised by X-ray photoelectron spectroscopy (XPS). XPS is a powerful technique used to investigate the electronic properties of the species formed on the surface and provides information about their chemical state in terms of quantitative effects. XPS allows us to define the binding energy of the atoms in the sample and describe the dependence between the shared electron pairs of individual atoms. This technique can identify any changes in binding energy values of electrons on the core–shell after any chemical changes in the atoms' backgrounds. As a consequence, XPS spectral peaks visibly shift with changes in energy; this chemical shift defines the types of chemical bindings between the atoms of the sample.

From the XPS data for the MCM-41, Ti-MCM-41, V-MCM-41 and Pd-MCM-41 samples shown in Fig. 8 and Table 3, the major peaks for MCM-41 include C 1s, N 1s, O 1s, and Si 2p signals at 284.98, 402.89, 532.78, and 103.38 eV, respectively. From the spectrum for Si photoelectrons from the 2p energy level, we can observe only one type of XPS signal with no shift in binding energy. For Si 2p, the binding energy of 103.38 eV suggests connections with oxygen by Si–O linkages in SiO_4^{4-} units. Similarly, the binding energy of O 1s (532.92 eV) suggests that its atoms are connected with silicon in the Si–O coupling.[55] XPS spectra were recorded for detailed investigation of the chemical states of the elements on the surface of Ti-MCM-41. The major peaks in the Ti-MCM-41 spectra for C 1S, N 1S, O 1s, Si 2p, and Ti 2p were observed at 285.03, 402.91, 532.92, 103.52 and 458.65 eV, respectively. The Ti 2p XPS spectra consisted of double peaks (Ti $2p_{1/2}$ and $2p_{3/2}$) for which the binding energies were 464.4 and 458.65 eV, respectively, characteristic of Ti^{4+}.[56] The rich Ti(IV) sites in the framework, which provide weak Lewis acid sites on the surface, and the mesoporous structure with large pore diameter are significant advantages for enhancing the catalytic properties of these Ti-MCM-41 materials. The binding energy of O 1s of Ti-MCM-41 sample presents only one intense peak at 532.92 eV, which corresponds to the O 1s of Si–O–Si linkages.[57] We further use XPS to evaluate the surface composition and chemical states of vanadium species. The major peaks in the V-MCM-41 spectra for C 1S, N 1S, O 1s, Si 2p, and V 2p are observed at 285.01, 402.76, 532.65, 103.21 and 516.60 eV, respectively. As shown in Fig. 8, the XPS spectrum of the V 2p region of the V-MCM-41 sample has a peak centred at 516.60 eV corresponding to V^{4+}.[58] The significant peaks in the Pd-MCM-41 spectra for C 1S, N 1S, O 1s, Si 2p, and Pd 3d are observed at 284.96, 402.84, 532.75, 103.36 and 335.93 eV, respectively. The XPS spectrum of Pd-MCM-41 exhibits two peaks at 337.8 and 342.2 eV, respectively assigned to Pd $3d_{3/2}$ and Pd $3d_{5/2}$, corresponding to Pd(II). The palladium species were bonded with one or two oxygen atoms to form Pd–O and –O–Pd–O– units.[59]

3.9. Anti-microbial and anti-cancer activity

Differential anti-microbial activity was displayed by MS, Ti-MS, V-MS and Pd-MS toward the four bacterial strains. Interestingly, Ti-MS (ZOI at 900 μg ml^{-1}: *E. coli* 15 mm and *S. paratyphi* 16 mm) and V-MS (ZOI at 900 μg ml^{-1}: *E. coli* 13 mm and *S. paratyphi* 22 mm) revealed extreme activity against Gram-negative bacteria while Pd-MS showed maximum activity toward Gram-positive bacteria (ZOI at 900 μg ml^{-1}: *B. subtilis* 17 mm and *S. aureus* 18 mm) (Table 4). However, MS does not display a significant difference in activity between Gram-positive and Gram-negative bacteria (Table 4). The excess deactivation varies with metal ion and is further supported by the surfactants and silicate species present in the as-synthesized molecular sieves. The antimicrobial activity occurs because the low lipophilicity causes the materials to not enter through the lipid membrane. Hence, the materials neither obstruct the metal-binding sites nor inhibit the growth of microbial enzymes.

Cell viability analysis revealed potent anti-cancer activity for MCM-41, Pd-MCM-41, V-MCM-41 and Ti-MCM-41 against three

Table 3 Quantitative results of XPS analysis for MCM-41, Ti-MCM-41, V-MCM-41 and Pd-MCM-41

Sample	Name	Peak BE	FWHM (eV)	Area (P) CPS (eV)	Atomic (%)
MCM-41	C 1s	284.98	1.55	72093.42	28.7
	N 1s	402.89	1.46	6572.36	1.7
	O 1s	532.78	1.72	292781.30	47.8
	Si 2p	103.38	1.79	55577.76	21.8
Ti-MCM-41	C 1s	285.03	1.50	74703.56	30.6
	N 1s	402.91	1.44	6158.36	1.6
	O 1s	532.92	1.68	280071.51	47.4
	Si 2p	103.52	1.76	49549.57	20.2
	Ti 2p	458.65	1.49	2770.97	0.2
V-MCM-41	C 1s	285.01	1.63	81171.40	32.4
	N 1s	402.76	1.41	6781.83	1.7
	O 1s	532.65	1.72	279816.12	46.2
	Si 2p	103.21	1.80	48319.89	19.2
	V 2p	516.60	2.76	11026.78	0.6
Pd-MCM-41	C 1s	284.96	1.54	62194.45	29.5
	N 1s	402.84	1.40	5860.61	1.8
	O 1s	532.75	1.69	242619.68	47.7
	Si 2p	103.36	1.78	44273.00	20.9
	Pd 3d	335.93	2.05	2817.48	0.1

Table 4 Anti-microbial activities of MS, Ti-MS, V-MS, and Pd-MS

S. no.	Name of the mesoporous material	Conc. (μg ml^{-1})	Zone of inhibition (in mm)			
			Escherichia coli	*Salmonella paratyphi*	*Bacillus subtilis*	*Staphylococcus aureus*
1	MS	600	7	8	9	9
		900	10	15	14	14
2	Ti-MS	600	8	11	10	8
		900	15	16	13	13
3	V-MS	600	9	15	6	3
		900	13	22	12	11
4	Pd-MS	600	9	9	12	15
		900	13	10	17	18
5	Standard (streptomycin)	50	18	18	18	18
		100	26	26	26	26

Table 5 Anti-cancer activity of various MS type molecular sieves

S. no.	Name of the mesoporous material	IC50 (μg mL^{-1})		
		HeLa	MCF7	K562
1	MS	7.3 ± 0.5	19 ± 1	21.3 ± 0.5
2	Pd-MS	10.6 ± 1.1	17.3 ± 2.0	7 ± 0
3	V-MS	6.3 ± 0.5	4.3 ± 0.5	10.6 ± 0.5
4	Ti-MS	11.6 ± 1.1	18.3 ± 0.5	4 ± 0
	Daunorubicin	0.18 ± 0.04 μM	0.39 ± 0.01 μM	0.2 ± 0.02 μM

cell lines, HeLa, MCF7 and K562. The activity of these four compounds varied according to the cell type tested. For example, MCM-41 displayed two-fold higher activity in cervical cancer cell line HeLa (IC50 = 7.3 ± 0.5) than in breast cancer cell line MCF7 (IC50 = 19 ± 1) and leukemic cell line K562 (IC50 = 21.3 ± 0.5) (Table 4). Pd-MCM-41 and Ti-MCM-41 were more active against K562 (IC50: Pd-MS = 7 ± 0, Ti-MS = 4 ± 0) than HeLa (IC50: Pd-MS = 10.6 ± 1.1, Ti-MS = 11.6 ± 1.1) and MCF7 (IC50: Pd-MS = 17.3 ± 2.0, Ti-MS = 18.3 ± 0.5) cell lines (Table 3). Interestingly, V-MS displayed more activity in HeLa (IC50 = 6.3 ± 0.5) and MCF7 (IC50 = 4.3 ± 0.5) cell lines than in the K562 (IC50 = 10.6 ± 0.5) cell line (Table 5). In agreement with cell viability data, these compounds also displayed significant morphological changes in both HeLa and MCF7 cell lines (Fig. 9).

Further, the results show that mesoporous materials containing transition metal ions exhibit useful anticancer activity after their large surface area to volume ratio provided appropriate association with a tumour cell, with direct penetration of mesoporous materials hooked on the cell wall causing membrane damage and cell death. The anticancer activity of palladium compounds is a direct result of their quick hydrolysis, but they cause more risk in biological fluids. This might lead to the necessary detachment, establishment of very reactive palladium species and disintegration before entering the cell, because the palladium species cannot attain the target disease cells.[60] The high oxidation state of Ti(IV) in titanium mesoporous compounds could inhibit oxidation in the body. The anticancer activity of the titanium-containing mesoporous materials is governed by lipophilicity and membrane penetrability, because they have to cross the hydrophobic cell membrane

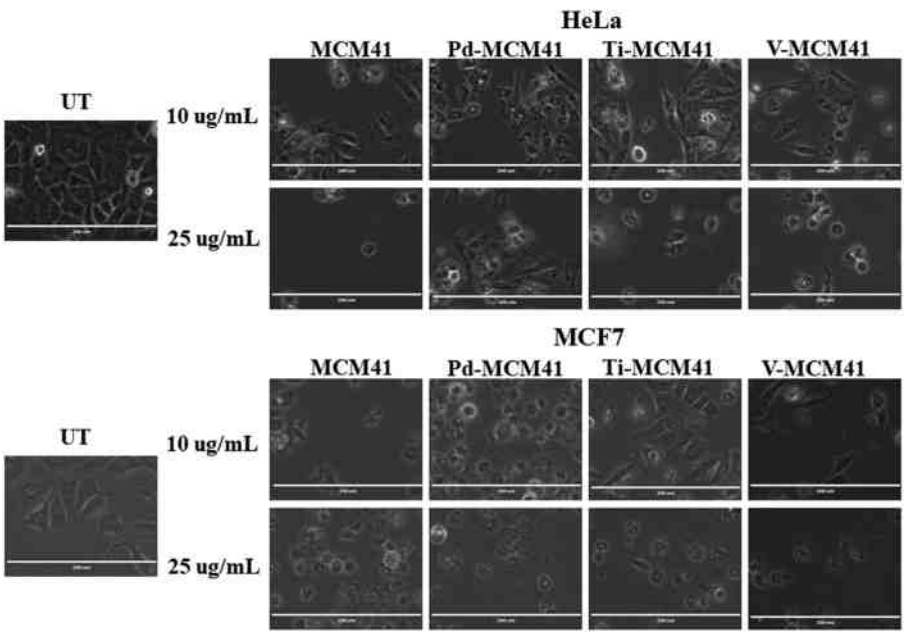

Fig. 9 Morphological changes in HeLa and MCF7 cell lines with various MS molecular sieves (MCM-41 = MS).

to reveal their biological activity. Earlier studies on pharmacokinetics showed that lipophilicity leads to enhanced penetrability across the cell membrane and causes better impact.[61–65] The open framework and neutral charge on the titanium mesoporous silica allows the passive dispersal of titanium ions into cancer cells, influencing the anticancer activity. Previous reports on anticancer activity stated that vanadium ions might intercalate with Lewis base sites of DNA base pairs and cause vanadium–DNA interactions. This results in passive diffusion of vanadium ions into the cancer cells and indicates anticancer activity. These studies signify that the vanadium mesoporous silica was effectively bound to the phosphate groups present in the nucleotides, which led to anticancer action.[66]

4. Conclusions

Novel mesoporous antimicrobial and anticancer molecular sieves containing Ti, V, and Pd were synthesised by a new procedure. Comparatively, this room temperature sol–gel synthesis is simpler in reaction conditions and lower in crystallisation time than the conventional hydrothermal method. The morphological and structural properties were studied in detail. The MS were found to possess potential antimicrobial and anticancer activity. A plausible mechanism for their biological activity was described. The transition-metal-containing mesoporous materials are highly helpful for biological applications as inert silica supports.

Conflicts of interest

There are no conflicts to declare.

Acknowledgements

The authors are thankful to the Department of Science and Technology-Science and Engineering Research Board (DST-SERB), New Delhi (EMR/2014/000629) for partial funding. CS, thanks to the Ministry of Human Resource Development (MHRD), New Delhi for a Senior Research Fellowship (SRF).

References

1 D. Saha, K. E. Warren and A. K. Naskar, Controlled release of antipyrine from mesoporous carbons, *Microporous Mesoporous Mater.*, 2014, **196**, 327–334, DOI: 10.1016/j.micromeso.2014.05.024.

2 M. Geszke-Moritz and M. Moritz, Quantum dots as versatile probes in medical sciences: Synthesis, modification and properties, *Mater. Sci. Eng., C*, 2013, **33**(3), 1008–1021, DOI: 10.1016/j.msec.2013.01.003.

3 A. Kaur and U. Gupta, A review on applications of nanoparticles for the preconcentration of environmental pollutants, *J. Mater. Chem.*, 2009, **19**(44), 8279, DOI: 10.1039/b901933b.

4 K. Dimos, P. Stathi, M. A. Karakassides and Y. Deligiannakis, Synthesis and characterization of hybrid MCM-41 materials for heavy metal adsorption, *Microporous Mesoporous Mater.*, 2009, **126**(1–2), 65–71, DOI: 10.1016/j.micromeso.2009.05.021.

5 X. Hu, B. O. Skadtchenko, M. Trudeau and D. M. Antonelli, Hydrogen Storage in Chemically Reducible Mesoporous and Microporous Ti Oxides, *J. Am. Chem. Soc.*, 2006, **128**(36), 11740–11741, DOI: 10.1021/ja0639766.

6 J. J. Williams, A. D. Wiersum, N. A. Seaton and T. Düren, Effect of Surface Group Functionalization on the CO2/N2 Separation Properties of MCM-41: A Grand-Canonical Monte Carlo Simulation Study, *J. Phys. Chem. C*, 2010, **114**(43), 18538–18547, DOI: 10.1021/jp105464u.

7 Y. Wan, H. Wang, Q. Zhao, M. Klingstedt, O. Terasaki and D. Zhao, Ordered Mesoporous Pd/Silica−Carbon as a Highly Active Heterogeneous Catalyst for Coupling Reaction of Chlorobenzene in Aqueous Media, *J. Am. Chem. Soc.*, 2009, **131**(12), 4541–4550, DOI: 10.1021/ja808481g.

8 K. Sarkar, K. Dhara, M. Nandi, P. Roy, A. Bhaumik and P. Banerjee, Selective Zinc(II)-Ion Fluorescence Sensing by a Functionalized Mesoporous Material Covalently Grafted with a Fluorescent Chromophore and Consequent Biological Applications, *Adv. Funct. Mater.*, 2009, **19**(2), 223–234, DOI: 10.1002/adfm.200800888.

9 Y. Wang, T. Brezesinski, M. Antonietti and B. Smarsly, Ordered Mesoporous Sb-, Nb-, and Ta-Doped SnO_2 Thin Films with Adjustable Doping Levels and High Electrical Conductivity, *ACS Nano*, 2009, **3**(6), 1373–1378, DOI: 10.1021/nn900108x.

10 S. Inagaki, O. Ohtani, Y. Goto, K. Okamoto, M. Ikai, K. Yamanaka and T. Okada, Light Harvesting by a Periodic Mesoporous Organosilica Chromophore, *Angew. Chem., Int. Ed.*, 2009, **48**(22), 4042–4046, DOI: 10.1002/anie.200900266.

11 D. Chandra, S. Mridha, D. Basak and A. Bhaumik, Template directed synthesis of mesoporous ZnO having high porosity and enhanced optoelectronic properties, *Chem. Commun.*, 2009, 2384, DOI: 10.1039/b901941c.

12 C. T. Kresge, M. E. Leonowicz, W. J. Roth, J. C. Vartuli and J. S. Beck, Ordered mesoporous molecular sieves synthesized by a liquid-crystal template mechanism, *Nature*, 1992, **359**(6397), 710–712, DOI: 10.1038/359710a0.

13 A. M. Sauer, A. Schlossbauer, N. Ruthardt, V. Cauda, T. Bein and C. Bräuchle, Role of Endosomal Escape for Disulfide-Based Drug Delivery from Colloidal Mesoporous Silica Evaluated by Live-Cell Imaging, *Nano Lett.*, 2010, **10**(9), 3684–3691, DOI: 10.1021/nl102180s.

14 A. López-Noriega, D. Arcos, I. Izquierdo-Barba, Y. Sakamoto, O. Terasaki and M. Vallet-Regí, Ordered Mesoporous Bioactive Glasses for Bone Tissue Regeneration, *Chem. Mater.*, 2006, **18**(13), 3137–3144, DOI: 10.1021/cm060488o.

15 J. Liu, A. Stace-Naughton, X. Jiang and C. J. Brinker, Porous Nanoparticle Supported Lipid Bilayers (Protocells) as Delivery Vehicles, *J. Am. Chem. Soc.*, 2009, **131**(4), 1354–1355, DOI: 10.1021/ja808018y.

16 M. P. Kapoor, A. Bhaumik, S. Inagaki, K. Kuraoka and T. Yazawa, Titanium containing inorganic–organic hybrid mesoporous materials with exceptional activity in epoxidation of alkenes using hydrogen peroxide, *J. Mater. Chem.*, 2002, **12**(10), 3078–3083, DOI: 10.1039/b204524a.

17 J. M. Rosenholm, C. Sahlgren and M. Lindén, Towards multifunctional, targeted drug delivery systems using mesoporous silica nanoparticles – opportunities & challenges, *Nanoscale*, 2010, **2**(10), 1870, DOI: 10.1039/c0nr00156b.

18 C.-H. Lee, S.-H. Cheng, I.-P. Huang, J. S. Souris, C.-S. Yang, C.-Y. Mou and L.-W. Lo, Intracellular pH-Responsive Mesoporous Silica Nanoparticles for the Controlled Release of Anticancer Chemotherapeutics, *Angew. Chem., Int. Ed.*, 2010, **49**(44), 8214–8219, DOI: 10.1002/anie.201002639.

19 H. Meng, M. Xue, T. Xia, Y.-L. Zhao, F. Tamanoi, J. F. Stoddart and A. E. Nel, Autonomous *in vitro* Anticancer Drug Release from Mesoporous Silica Nanoparticles by pH-Sensitive Nanovalves, *J. Am. Chem. Soc.*, 2010, **132**(36), 12690–12697, DOI: 10.1021/ja104501a.

20 Z. Tao, B. Toms, J. Goodisman and T. Asefa, Mesoporous Silica Microparticles Enhance the Cytotoxicity of Anticancer Platinum Drugs, *ACS Nano*, 2010, **4**(2), 789–794, DOI: 10.1021/nn9015345.

21 Y. Chen, H. Chen, S. Zhang, F. Chen, L. Zhang, J. Zhang and J. Shi, Multifunctional Mesoporous Nanoellipsoids for Biological Bimodal Imaging and Magnetically Targeted Delivery of Anticancer Drugs, *Adv. Funct. Mater.*, 2010, **21**(2), 270–278, DOI: 10.1002/adfm.201001495.

22 H. Meng, M. Liong, T. Xia, Z. Li, Z. Ji, J. I. Zink and A. E. Nel, Engineered Design of Mesoporous Silica Nanoparticles to Deliver Doxorubicin and P-Glycoprotein siRNA to Overcome Drug Resistance in a Cancer Cell Line, *ACS Nano*, 2010, **4**(8), 4539–4550, DOI: 10.1021/nn100690m.

23 N. Summerlin, Z. Qu, N. Pujara, Y. Sheng, S. Jambhrunkar, M. McGuckin and A. Popat, Colloidal mesoporous silica nanoparticles enhance the biological activity of resveratrol, *Colloids Surf., B*, 2016, **144**, 1–7, DOI: 10.1016/j.colsurfb.2016.03.076.

24 S. Baek, R. K. Singh, D. Khanal, K. D. Patel, E.-J. Lee, K. W. Leong and H.-W. Kim, Smart multifunctional drug delivery towards anticancer therapy harmonized in mesoporous nanoparticles, *Nanoscale*, 2015, **7**(34), 14191–14216, DOI: 10.1039/c5nr02730f.

25 K. M. Parida and S. S. Dash, Manganese containing MCM-41: synthesis, characterization and catalytic activity in the oxidation of ethylbenzene, *J. Mol. Catal. A: Chem.*, 2009, **306**(1–2), 54–61, DOI: 10.1016/j.molcata.2009.02.022.

26 S. P. Naik, A. S. T. Chiang and R. W. Thompson, Synthesis of Zeolitic Mesoporous Materials by Dry Gel Conversion under Controlled Humidity, *J. Phys. Chem. B*, 2003, **107**(29), 7006–7014, DOI: 10.1021/jp034425u.

27 B. G. Trewyn, I. I. Slowing, S. Giri, H.-T. Chen and V. S.-Y. Lin, Synthesis and Functionalization of a Mesoporous Silica Nanoparticle-Based on the Sol–Gel Process and Applications in Controlled Release, *Acc. Chem. Res.*, 2007, **40**(9), 846–853, DOI: 10.1021/ar600032u.

28 X. Yang, S. Zhang, Z. Qiu, G. Tian, Y. Feng and F.-S. Xiao, Stable Ordered Mesoporous Silica Materials Templated by High-Temperature Stable Surfactant Micelle in Alkaline Media, *J. Phys. Chem. B*, 2004, **108**(15), 4696–4700, DOI: 10.1021/jp0380226.

29 M. A. Karakassides, A. Bourlinos, D. Petridis, L. Coche-Guerènte and P. Labbè, Synthesis and characterization of copper containing mesoporous silicas, *J. Mater. Chem.*, 2000, **10**(2), 403–408, DOI: 10.1039/a904545g.

30 V. R. Elías, M. E. Crivello, E. R. Herrero, S. G. Casuscelli and G. A. Eimer, Some considerations to optimize the synthesis procedure and the structural quality of mesostructured silica, *J. Non-Cryst. Solids*, 2009, **355**(22–23), 1269–1273, DOI: 10.1016/j.jnoncrysol.2009.04.019.

31 F. Schüth, Non-siliceous Mesostructured and Mesoporous Materials†, *Chem. Mater.*, 2001, **13**(10), 3184–3195, DOI: 10.1021/cm011030j.

32 J. N. Kondo and K. Domen, Crystallization of Mesoporous Metal Oxides†, *Chem. Mater.*, 2008, **20**(3), 835–847, DOI: 10.1021/cm702176m.

33 S. K. Das, M. K. Bhunia, D. Chakraborty, A. R. Khuda-Bukhsh and A. Bhaumik, Hollow spherical mesoporous phosphosilicate nanoparticles as a delivery vehicle for an antibiotic drug, *Chem. Commun.*, 2012, **48**(23), 2891, DOI: 10.1039/c2cc17181c.

34 T.-W. Sun, Y.-J. Zhu, C. Qi, F. Chen, Y.-Y. Jiang, Y.-G. Zhang and C. Wu, Templated solvothermal synthesis of magnesium silicate hollow nanospheres with ultrahigh specific surface area and their application in high-performance protein adsorption and drug delivery, *J. Mater. Chem. B*, 2016, **4**(19), 3257–3268, DOI: 10.1039/c5tb02632f.

35 N. Pal and A. Bhaumik, Soft templating strategies for the synthesis of mesoporous materials: Inorganic, organic–inorganic hybrid and purely organic solids, *Adv. Colloid Interface Sci.*, 2013, **189–190**, 21–41, DOI: 10.1016/j.cis.2012.12.002.

36 A. Rajini, A. K. Adepu, S. Chirra and N. Venkatathri, Titanium aminophosphates: synthesis, characterization, antimicrobial and cytotoxicity studies, *RSC Adv.*, 2015, **5**(106), 87713–87722, DOI: 10.1039/c5ra15084a.

37 A. Rajini, M. Nookaraju, I. A. K. Reddy and N. Venkatathri, Synthesis, characterization, antimicrobial and cytotoxicity studies of a novel titanium dodecylamino phosphate, *J. Saudi Chem. Soc.*, 2017, **21**, S77–S85, DOI: 10.1016/j.jscs.2013.10.005.

38 A. Rajini, M. Nookaraju, N. Venkatathri and I. A. K. Reddy, Synthesis, characterization, antimicrobial and cytotoxic studies of a novel vanadium dodecylamino phosphate, *Arabian J. Chem.*, 2017, **10**, S2082–S2089, DOI: 10.1016/j.arabjc.2013.07.038.

39 A. Rajini, A. K. Adepu, S. Chirra and N. Venkatathri, Porous palladium aminophosphates: synthesis, characterization, antimicrobial and cytotoxicity studies, *RSC Adv.*, 2015, **5**(82), 66956–66964, DOI: 10.1039/c5ra11923e.

40 J. S. Beck, J. C. Vartuli, W. J. Roth, M. E. Leonowicz, C. T. Kresge, K. D. Schmitt and J. L. Schlenker, A new family of mesoporous molecular sieves prepared with liquid crystal templates, *J. Am. Chem. Soc.*, 1992, **114**(27), 10834–10843, DOI: 10.1021/ja00053a020.

41 C. T. Kresge, M. E. Leonowicz, W. J. Roth, J. C. Vartuli and J. S. Beck, Ordered mesoporous molecular sieves synthesized by a liquid-crystal template mechanism, *Nature*, 1992, **359**(6397), 710–712, DOI: 10.1038/359710a0.

42 K. Shiva Kumar, M. Siddi Ramulu, B. Rajesham, N. P. Kumar, V. Voora and R. K. Kancha, $FeCl_3$ catalysed

7-membered ring formation in a single pot: a new route to indole-fused oxepines/azepines and their cytotoxic activity, *Org. Biomol. Chem.*, 2017, **15**(20), 4468–4476, DOI: 10.1039/c7ob00715a.

43 J. M. Rosenholm, C. Sahlgren and M. Lindén, Towards multifunctional, targeted drug delivery systems using mesoporous silica nanoparticles – opportunities & challenges, *Nanoscale*, 2010, **2**(10), 1870, DOI: 10.1039/c0nr00156b.

44 C.-H. Lee, S.-H. Cheng, I.-P. Huang, J. S. Souris, C.-S. Yang, C.-Y. Mou and L.-W. Lo, Intracellular pH-Responsive Mesoporous Silica Nanoparticles for the Controlled Release of Anticancer Chemotherapeutics, *Angew. Chem., Int. Ed.*, 2010, **49**(44), 8214–8219, DOI: 10.1002/anie.201002639.

45 S. V. Awate, N. E. Jacob, S. S. Deshpande, T. R. Gaydhankar and A. A. Belhekar, Synthesis, characterization and photocatalytic degradation of aqueous eosin over Cr containing Ti/MCM-41 and SiO_2–TiO_2 catalysts using visible light, *J. Mol. Catal. A: Chem.*, 2005, **226**(2), 149–154, DOI: 10.1016/j.molcata.2004.09.055.

46 L. Li, P. Wu, Q. Yu, G. Wu and N. Guan, Low-temperature H2-SCR over platinum catalysts supported on Ti-containing MCM-41, *Appl. Catal., B*, 2010, **94**(3–4), 254–262, DOI: 10.1016/j.apcatb.2009.11.016.

47 S.-W. Song, K. Hidajat and S. Kawi, Functionalized SBA-15 Materials as Carriers for Controlled Drug Delivery: Influence of Surface Properties on Matrix–Drug Interactions, *Langmuir*, 2005, **21**(21), 9568–9575, DOI: 10.1021/la051167e.

48 P. Horcajada, A. Rámila, J. Pérez-Pariente and M. Vallet-Regí, Influence of pore size of MCM-41 matrices on drug delivery rate, *Microporous Mesoporous Mater.*, 2004, **68**(1–3), 105–109, DOI: 10.1016/j.micromeso.2003.12.012.

49 S. Chirra and N. Venkatathri, A novel method of synthesis and a new insight into the vanadium incorporation in three dimensional mesoporous KIT-6, *Mater. Res. Express*, 2018, **6**(1), 15021, DOI: 10.1088/2053-1591/aae45d.

50 Z. A. Alothman and A. W. Apblett, Metal ion adsorption using polyamine-functionalized mesoporous materials prepared from bromopropyl-functionalized mesoporous silica, *J. Hazard. Mater.*, 2010, **182**(1–3), 581–590, DOI: 10.1016/j.jhazmat.2010.06.072.

51 Z. ALOthman, A Review: Fundamental Aspects of Silicate Mesoporous Materials, *Materials*, 2012, **5**(12), 2874–2902, DOI: 10.3390/ma5122874.

52 S. Chirra, S. Siliveri, A. K. Adepu, S. Goskula, S. R. Gujjula and V. Narayanan, Pd-KIT-6: synthesis of a novel three-dimensional mesoporous catalyst and studies on its enhanced catalytic applications, *J. Porous Mater.*, 2019, DOI: 10.1007/s10934-019-00763-5.

53 K. Song, J. Guan, Z. Wang, C. Xu and Q. Kan, Post-treatment of mesoporous material with high temperature for synthesis super-microporous materials with enhanced hydrothermal stability, *Appl. Surf. Sci.*, 2009, **255**(11), 5843–5846, DOI: 10.1016/j.apsusc.2009.01.016.

54 K. M. Parida and S. S. Dash, Manganese containing MCM-41: synthesis, characterization and catalytic activity in the oxidation of ethylbenzene, *J. Mol. Catal. A: Chem.*, 2009, **306**(1–2), 54–61, DOI: 10.1016/j.molcata.2009.02.022.

55 A. Sterczyńska, A. Deryło-Marczewska, M. Zienkiewicz-Strzałka, M. Śliwińska-Bartkowiak and K. Domin, Surface Properties of Al-Functionalized Mesoporous MCM-41 and the Melting Behavior of Water in Al-MCM-41 Nanopores, *Langmuir*, 2017, **33**(42), 11203–11216, DOI: 10.1021/acs.langmuir.7b02172.

56 B. M. Reddy, K. N. Rao, G. K. Reddy and P. Bharali, Characterization and catalytic activity of V_2O_5/Al_2O_3–TiO_2 for selective oxidation of 4-methylanisole, *J. Mol. Catal. A: Chem.*, 2006, **253**(1–2), 44–51, DOI: 10.1016/j.molcata.2006.03.016.

57 S. Wang, Y. Shi and X. Ma, Microwave synthesis, characterization and transesterification activities of Ti-MCM-41, *Microporous Mesoporous Mater.*, 2012, **156**, 22–28, DOI: 10.1016/j.micromeso.2012.02.011.

58 W. Qian, H. Wang, J. Chen and Y. Kong, Spherical V-Fe-MCM-48: The Synthesis, Characterization and Hydrothermal Stability, *Materials*, 2015, **8**(4), 1752–1765, DOI: 10.3390/ma8041752.

59 C. Sener, T. Dogu and G. Dogu, Effects of synthesis conditions on the structure of Pd incorporated MCM-41 type mesoporous nanocomposite catalytic materials with high Pd/Si ratios, *Microporous Mesoporous Mater.*, 2006, **94**(1–3), 89–98, DOI: 10.1016/j.micromeso.2006.03.026.

60 C. Navarro-Ranninger, I. LóPez-Solera, J. M. Pérez, J. R. Masaguer and C. Alonso, *In vitro* antitumour activity of two isomeric cyclopalladiated compounds derived from benzoylbenzylidenimines, *Appl. Organomet. Chem.*, 1993, **7**(1), 57–61, DOI: 10.1002/aoc.590070107.

61 N. W. Schmidt and G. C. L. Wong, Antimicrobial peptides and induced membrane curvature: geometry, coordination chemistry, and molecular engineering, *Curr. Opin. Solid State Mater. Sci.*, 2013, **17**(4), 151–163, DOI: 10.1016/j.cossms.2013.09.004.

62 S. Szunerits and R. Boukherroub, Antibacterial activity of graphene-based materials, *J. Mater. Chem. B*, 2016, **4**(43), 6892–6912, DOI: 10.1039/c6tb01647b.

63 D. Irby, C. Du and F. Li, Lipid–Drug Conjugate for Enhancing Drug Delivery, *Mol. Pharmaceutics*, 2017, **14**(5), 1325–1338, DOI: 10.1021/acs.molpharmaceut.6b01027.

64 A. C. Alves, D. Ribeiro, C. Nunes and S. Reis, Biophysics in cancer: the relevance of drug–membrane interaction studies, *Biochim. Biophys. Acta, Biomembr.*, 2016, **1858**(9), 2231–2244, DOI: 10.1016/j.bbamem.2016.06.025.

65 C. Pampillón, J. Claffey, K. Strohfeldt and M. Tacke, Synthesis and cytotoxicity studies of new dimethylamino-functionalised and aryl-substituted titanocene anti-cancer agents, *Eur. J. Med. Chem.*, 2008, **43**(1), 122–128, DOI: 10.1016/j.ejmech.2007.02.011.

66 A. Bishayee, A. Waghray, M. A. Patel and M. Chatterjee, Vanadium in the detection, prevention and treatment of cancer: the *in vivo* evidence, *Cancer Lett.*, 2010, **294**(1), 1–12, DOI: 10.1016/j.canlet.2010.01.030.